Surface-plasmon field-enhanced multiphoton photoelectric emission from metal films

T. Tsang, T. Srinivasan-Rao, and J. Fischer
Brookhaven National Laboratory, Upton, New York 11973
(Received 29 June 1990)

We report a study of surface-plasmon-mediated multiphoton photoelectric emission from thin films of Ag, Au, Cu, and Al. The experiments were performed in the Kretchmann attenuated-total-internal reflection geometry while the excitation source was an unamplified femtosecond colliding-pulse mode-locked ring laser. Contrast to the electron emission obtained by irradiating the laser on a metal surface, electron yield increases by several orders of magnitude with fairly high quantum efficiency, is observed when photons are coupled to the surface-plasmon modes of these films. Although the photon absorption reaches its maximum when the reflectivity exhibits a deep minimum at the surface-plasmon resonance angle, it is found that the maximum electron yield occurs at a slightly different angle than the reflectivity dip. The results of these measurements favor the field-density calculations using the Fresnel equations. The width of the electron temporal profile, measured utilizing this nonlinear photoelectric effect, however, fails to show the narrowing commensurate with the higher-order nonlinearity.

I. INTRODUCTION

Surface-plasmon- (SP) mediated enhancement phenomena such as second-harmonic generation,[1,2] hot-electron generation,[3] Brillouin scattering,[4,5] Raman scattering,[6] photoconductivity in metal-oxide-metal tunnel junctions,[7,8] and optical bistability[9,10] occurring at surfaces of thin metal films have been examined for the past decade. Linear photoelectric emission mediated via the SP from thin films of cesium-enriched Ag and Al has also been investigated,[11–14] but no systematic study has been performed. Recently, we have demonstrated the surface-plasmon-enhanced nonlinear photoelectric emission from a thin silver film,[15] where the electron yield was increased by 5×10^3 over that of the bulk emission measured for the same film at the same power fluence. In this study, we present a detailed investigation of the multiphoton photoelectric emission mediated by the SP in other metal films. This systematic study leads us to conclude that electrons emitted via the SP are most likely due to the enhanced electromagnetic field density localized at the metal-vacuum interface rather than the increased absorption at the SP resonance, and the nonlinearity arises from the coupling between the SP to the single-electron state.

Our interest in the multiphoton photoelectric emission[16–19] via SP excitation is to examine the possibility of the nonlinear photoemission overtaking the linear photoemission process so that a higher quantum efficiency and higher brightness electron source can be obtained from metal cathode photoinjectors. Recent investigations of electron emission employing the surface photoelectric effect[20–22] have proven that the electron yield can be enhanced by a factor of ~10 with p-polarized light. Since SP field densities are strongly confined to the metal-vacuum interface to within a few Thomas-Fermi wavelengths, electrons emitted due to this high-field density could result in a higher yield than those emitted via the conventional surface photoelectric effect.

The outline of the paper is as follows. In Sec. II a brief description of the SP generation, dispersion relation, field density calculations based on classical electromagnetic theory, and the theoretical model of the linear and the nonlinear photoelectric emission process are given. In Sec. III the detailed experimental conditions are given. In Sec. IV the experimental results and the comparison with the surface-plasmon field density calculations are presented. Finally, we draw our conclusions in Sec. V.

II. SP GENERATION, FIELD ENHANCEMENT, AND PHOTOEMISSION

A. SP generation

Because of the lack of the conservation of energy and wave vector, direct coupling between photon and SP is forbidden. However, in this experiment, we employ the well-known Kretchmann configuration for the generation of the SP.[23] Figure 1(a) shows the scheme of the attenuated-total-internal-reflection (ATR) technique. A thin metal film is thermally evaporated onto the hypotenuse side of a BK7 glass prism ($n=1.5154$ at 625 nm). A p-polarized laser beam irradiates at an angle of θ at the metal-glass interface from the glass side. After passing through the critical angle, the photon field couples to the SP via the evanescent field, which converts the transverse electromagnetic photon field into a mixture of transverse and longitudinal SP fields at the metal-vacuum interface. The momentum matching condition can be satisfied when the parallel component of the photon wave vector k_x, extended by the glass prism, matches that of the SP. By varying the incident angle θ, photon coupling to the SP can be evidenced by a drop of the reflected laser intensity. After including the frequency dependence of the dielectric constant for a metal from the Drude expression $\epsilon_1=1-\omega_p^2/\omega^2$, the dispersion curve

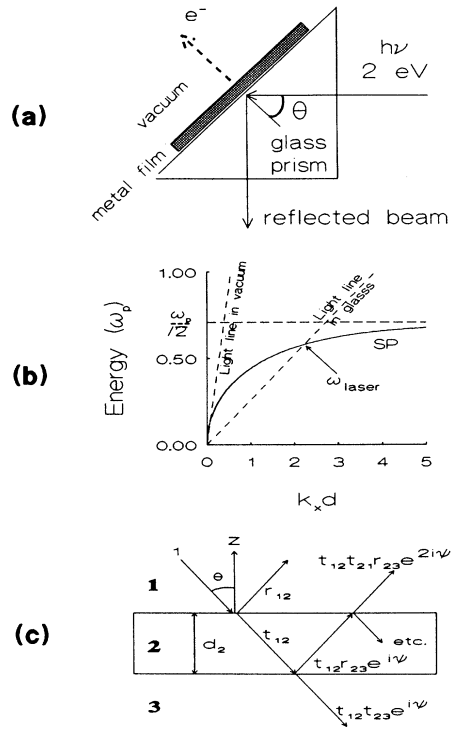

FIG. 1. (a) Kretchmann ATR geometry. (b) SP dispersion curve. (c) Three-layered dielectric structure.

$$k_x = \frac{\omega}{c}\left[\frac{\epsilon_1\epsilon_2}{\epsilon_1+\epsilon_2}\right]^{1/2} \tag{1}$$

is then plotted in Fig. 1(b).

According to this scenario, changing the angle of incidence would bend the laser light line in vacuum to cross the SP curve until conservation of energy is fulfilled. At the SP resonance angle θ_{SP}, the photon field will couple linearly to the SP mode at the metal-vacuum interface. Since the high-field density occurs at the surface of the metal, the emission of electrons suffering no electron-electron collision could be made possible.

B. Field enhancement

The field enhancement at the metal-vacuum interface can be calculated with the Fresnel reflection and transmission coefficients. Figure 1(c) illustrates the notations used. The Fresnel reflection R_{123} and transmission T_{123} coefficients for the three-layered structure are

$$R_{123} = \frac{r_{12}+r_{23}e^{2i\Psi}}{1+r_{12}r_{23}e^{2i\Psi}}\ , \tag{2}$$

$$T_{123} = \frac{t_{12}t_{23}e^{i\Psi}}{1+r_{12}r_{23}e^{2i\Psi}}\ , \tag{3}$$

where $\Psi = k_{2z}d_2$ and $k_{iz} = (\omega/c)(\epsilon_i - \epsilon_1\sin^2\theta_1)^{1/2}$. For p-polarization, the single-interface Fresnel coefficients between media i and j are

$$r_{ij} = \frac{\epsilon_j k_{iz} - \epsilon_i k_{jz}}{\epsilon_j k_{iz} + \epsilon_i k_{jz}}\ ,$$

$$t_{ij} = \frac{2\epsilon_i k_{iz}}{\epsilon_j k_{iz} + \epsilon_i k_{jz}}\ ,$$

where ϵ_i and ϵ_j are the dielectric constants. For s polarization, the indices permuted as $[ii]$ and $[jj]$ instead of $[ij]$ and $[ji]$. The absolute values of the coefficients R_{123} and T_{123} are the ratio of the amplitudes of the backward- and forward-traveling electromagnetic field to that of the incident field, respectively. Calculations of the enhanced electron yield based on photon absorption would require one to take the ratio of R_{123} to R_{321}, where media 1, 2, and 3 are glass, metal, and vacuum, respectively. However, when electron-yield enhancement is calculated based on the work done by the photons on the metals, one must consider the ratio of the fields E_{122} to E_{32}, which are located at the *metal side* of the metal-vacuum interface for the cases of SP resonance and nonresonance, respectively, where

$$E_{122} \equiv E_{SP} = \frac{t_{12}(1+r_{23})e^{i\Psi}}{1+r_{12}r_{23}e^{2i\Psi}}\ , \tag{4}$$

$$E_{32} \equiv E_{\neq SP} = \frac{t_{32}(1+r_{21}e^{2i\Psi})}{1+r_{32}r_{21}e^{2i\Psi}}\ , \tag{5}$$

while E_{SP} and $E_{\neq SP}$ correspond to the reflected field at the SP resonance and the transmitted field for the nonresonance case, respectively. This comparison can be made when the p-polarized laser beam irradiates the metal film from the vacuum side onto the metal film at the same incident angle, hence the nonresonance case.

The resonance of the SP field occurs when the laser field exerts work done on the current density of the metal film. At optical frequencies, the small damping (because of the small imaginary component of the dielectric constant) in noble metals results in a larger SP field. However, like all driven oscillators, the phase of the polarization field always lags behind the phase of the driving field.[24] Hence the resonance angle exhibited by the reflectivity measurement is not the same as the resonance angle shown by the maximum amplitude of the SP field. Details of this phenomenon has been examined theoretically[25–27] and experimentally[14] by several investigators. In this experiment, electron emission via the SP also serves uniquely to support this hypothesis by comparing the resonance angle registered by the minima of the ATR spectra to their corresponding electron-emission maxima.

C. Photoelectric effect—linear and nonlinear

The generalized Fowler-Dubridge theory[28] is used to interpret the results of our experiments. Within the context of this phenomenological theory, electron emission is the result of the partial current densities contributed by all higher-order processes. One can write the total current density as

$$J = \sum_{n=0}^{\infty} J_n\ , \tag{6}$$

where

$$J_n = a_n A \left[\frac{e}{h\nu}\right]^n I^n (1-R_{ijk})^n T^2 F\left[\frac{nh\nu-\phi}{kT}\right] \equiv b_n I^n . \tag{7}$$

The order of the multiphoton process is denoted by n, a_n is an experimentally determined constant which contains the transition matrix elements and the electron escape probability, A is the theoretical Richardson constant equal to 120 $A/cm^2 K^2$, e is the electron charge, $h\nu$ is the photon energy, ϕ is the work function, T is the absolute temperature of the sample, I is the incident laser intensity, k is Boltzmann's constant, R_{ijk} is the reflectivity of the three-layered structure, b_n is the nonlinear coefficient, and F is the Fowler function given by

$$F(x) = \begin{cases} \sum_{n=1}^{\infty} (-1)^{n+1} \dfrac{e^{nx}}{n^2}, & x \le 0 \\ \dfrac{\pi^2}{6} + \dfrac{x^2}{2} - \sum_{n=1}^{\infty} (-1)^{n+1} \dfrac{e^{-nx}}{n^2}, & x \ge 0 . \end{cases}$$

The first term of Eq. (6),

$$J_0 = a_0 A T^2 e^{-\phi/kT} , \tag{8}$$

is the thermionic emission, while the second term,

$$J_1 = a_1 A \left[\frac{e}{h\nu}\right] I(1-R) T^2 F\left[\frac{h\nu-\phi}{kT}\right] , \tag{9}$$

is the linear photoemission. It is worth pointing out that, according to Eq. (6), electron currents contributed by higher-order nonlinear processes do exist, but with negligible effect, even though only linear or thermionic processes are invoked. Vice versa, diminutive contributions due to linear and thermionic emission also exist when multiphoton processes are explored.

When electron-yield calculations based on the change of the absorption are considered, one would compare the enhancement by taking the ratio of the J_n for the SP resonance to that of the nonresonance case. Since the material constants denoted by Eq. (7) are identical for the SP resonance and the nonresonance case, therefore, when comparisons are made based only on the absorption, the ratio of the final electron current output density is given by

$$\left[\frac{(J_n)_{SP}}{(J_n)_{\neq SP}}\right]_{absorption} = \left[\frac{1-R_{123}}{1-R_{321}}\right]^n . \tag{10}$$

However, for the SP-mediated nonlinear photoemission it is the plasmon field rather than the much smaller $[I(1-R_{123})]^n$ phenomenological absorption that causes the ejection of electrons. Therefore it is conceivable that one should replace this absorption term by the *total* (incident plus reflected) SP electromagnetic field that is localized at the metal side of the metal-vacuum interface. This ratio is then given by

$$\left[\frac{(J_n)_{SP}}{(J_n)_{\neq SP}}\right]_{field} = \left|\frac{E_{122}+E_{12}e^{i\Psi}}{E_{32}+E_{322}e^{i\Psi}}\right|^{2n} , \tag{11}$$

where E_{322} and E_{12} are the reflected fields from the opposite interface to the metal-vacuum boundary. They are also given by Eqs. (4) and (5), respectively, but with different indices. In Sec. IV a comparison between Eqs. (10) and (11) with the data will be made.

III. EXPERIMENTAL DETAILS

The metal films used in this study are Ag, Au, Al, and Cu, their thickness are 475, 455, 110, and 430 Å, respectively. These thicknesses are obtained from fitting the Fresnel coefficients to the experimental ATR spectra. The thin films are thermally evaporated from 99.99% pure metal wires under a vacuum of 10^{-6} Torr. All films were exposed to air (less than 10 h) so that electrical connections would be made. Each sample is then inserted in a separate experimental chamber and pumped down to a vacuum of 10^{-9} Torr with proper degasing and baking.

The laser source is an unamplified colliding-pulse mode-locked (CPM) laser pumped by a 4-W all lines output of an Ar-ion laser. The dye laser optical pulse train has a repetition rate of 89.5 MHz with a pulse duration of 90 fs at 625 nm. Figure 2 shows the schematic of the experimental details. After passing through a combination of $\lambda/2$ wave plates and polarizer, the p-polarized laser beam is focused to a spot size of $\sim 5\times10^{-5}$ cm^2 using a 15-cm focusing lens, and irradiates the metal film from the glass side at the SP resonance angle $\sim 43°$. The first $\lambda/2$ wave plate and the polarizer act as a variable at-

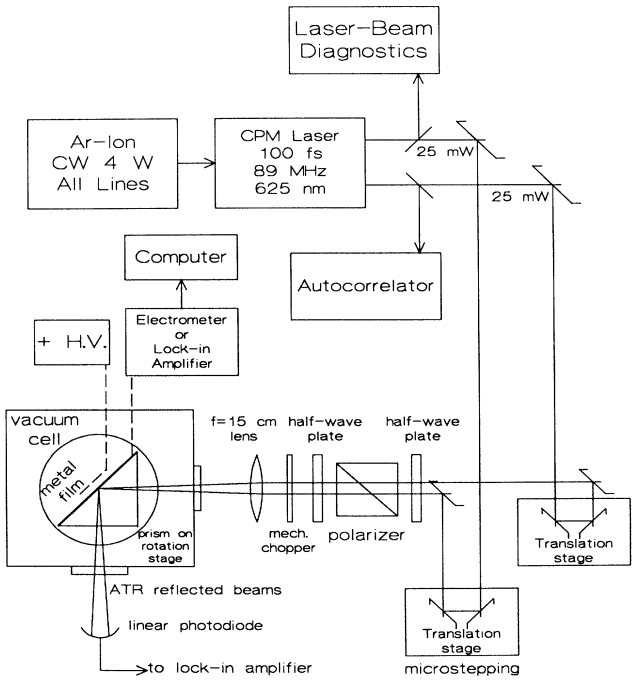

FIG. 2. Experimental arrangement for the SP-enhanced multiphoton photoelectric emission from metal films.

tenuator to facilitate the intensity-dependent measurements, while the second $\lambda/2$ wave plate varies the input polarization of the incidence beam from p to s so that the SP field can be varied from full thrust to zero. An extraction voltage of 1 kV is applied to a copper anode ring held $\sim$ 3 mm in front of the metal film to eliminate the space-charge effect. The quasi-dc current leaving the metal film is detected by an electrometer. Alternatively, lock-in technique has also been used to avoid residual dc background. Results from both techniques are in reasonable agreement. After digitization, the data are then stored in a computer for further analysis.

The ATR spectrum and the electron emission are monitored simultaneously when the incident angle of the laser beam is varied using a rotation stage. Although the exact angles of incidence are calibrated against the reflection off the normal incidence on the hypotenuse surface, the accuracy of the rotation stage limits the resolution to $\pm 0.5°$. However, the reflectance and the electron current are registered simultaneously; therefore the relative angle between both spectra are accurate to within $\pm 0.06°$.

The work functions of the metal films are measured using a Xe-Hg white-light source. Each output line of the Xe-Hg source is selected by a monochromater with a bandwith of 2.4 nm. Electron current output from each Xe-Hg line is normalized with respect to the response from a pyroelectric detector.

A programmable 0.1-μm resolution microstepping translation stage synchronized with the detection system is used to measure the electron temporal profile using the multiphoton photoelectric emission. In this experiment, both output beams from the CPM laser are employed to irradiate and resonantly couple to the SP modes. These beams are propagated collinearly, but were spatially offset vertically by a two-beam diameter before entering the focusing lens. Therefore, after final focusing both beams are capable of generating the SP. When the beams are spatially and temporally overlapped, electron emission due to higher-order processes would occur.

IV. RESULTS AND ANALYSIS

A. ATR and electron-emission spectra

Full analysis of the SP requires a theoretical fit to an experimental ATR spectrum obtained from a well-collimated monochromatic light source, so that the precise metal dielectric constants and film thickness can be derived. Figure 3 shows the experimentally and theoretically fitted p- and s-polarized ATR spectra for a well-collimated (unfocused) He-Ne laser. The dielectric constants for the fitted spectra displayed in each figure are in good agreement with the literature values.[29] The residual reflectance at the SP resonance angles, 42.89° for Ag, 44.18° for Au, 44.31° for Al, and 43.06° for Cu, are due to the unoptimized film thickness. From these results, it is clear that s-polarized light does not couple to the SP mode.

Figure 4 shows the experimental p- and s-polarized ATR spectra and their corresponding normalized electron yield for all four metal films when the focused CPM

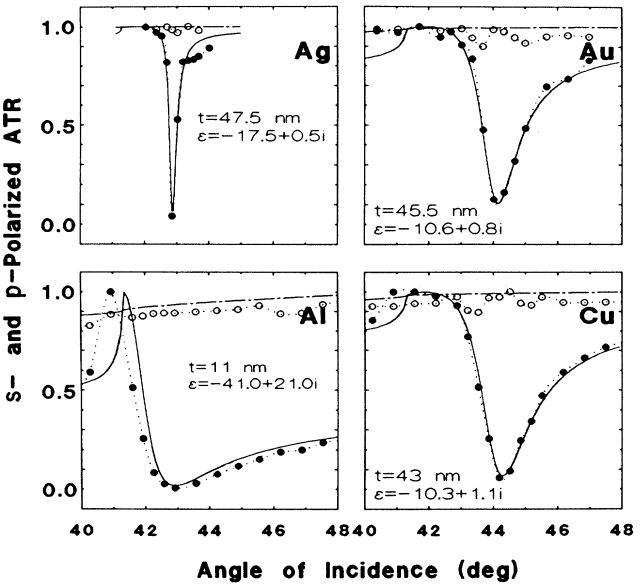

FIG. 3. Theoretical fitted p (——) and s (–·–) polarization, and the experimental p (●) and s (○) values of the ATR spectra for thin films of Ag, Au, Al, and Cu using a well-collimated He-Ne laser. Data points are connected with dotted lines for clarity.

laser beam is used. The simultaneous absence of both the SP reflectivity dips and the electron-emission peaks with s-polarized laser beams are distinctively noticeable. Also, the width of the electron peaks, in all cases, are narrower than their ATR dips, indicating the presence of the nonlinear process. With the exception of Ag, all p-polarized

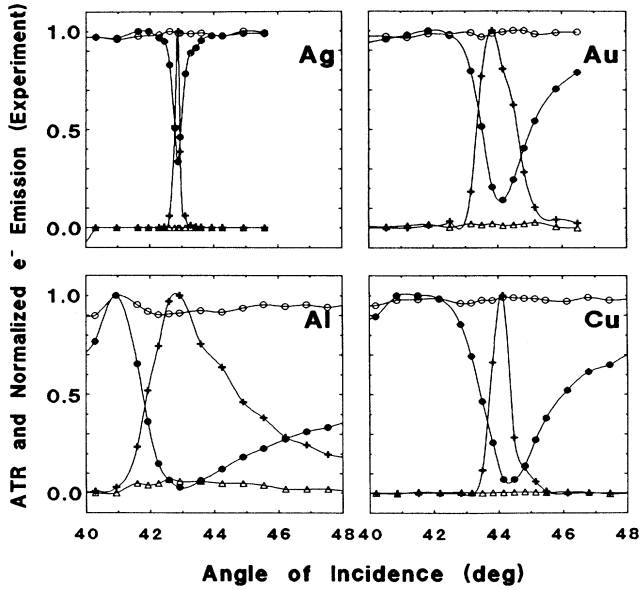

FIG. 4. Experimental values of the p (●) and the s (○) polarized ATR spectra using a femtosecond CPM laser. The corresponding normalized p (+) and s (△) polarized electron emissions are also presented.

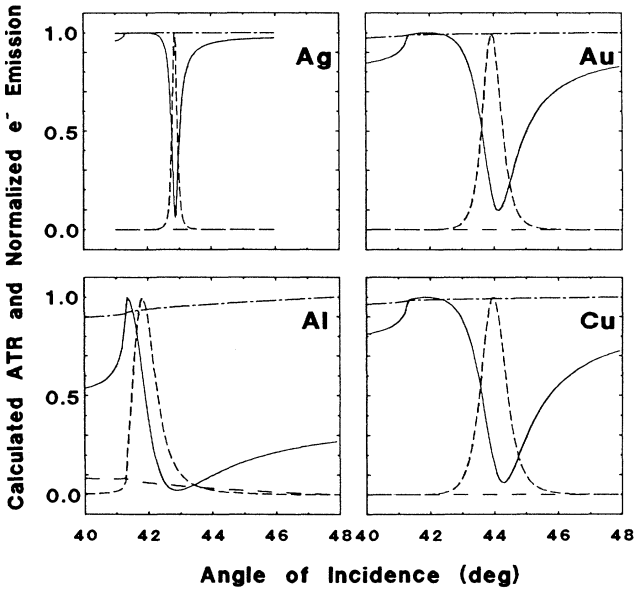

FIG. 5. Theoretical fitted p (——) and s (–·–) polarized ATR spectra. The corresponding calculated p (— —) and s (---) polarized field densities raised to the power $2n$ are also illustrated.

ATR spectra depicted in Fig. 4 reach ~0.1 at the SP resonance angles. The discrepancy for the Ag film can be understood by comparing the ATR spectra of the *collimated* He-Ne laser (Fig. 3) to that of the *focused* CPM laser (Fig. 4). Since the efficient coupling of the photon field to SP depends critically on the purity of the $k_x = k_{\text{laser}} \sin\theta$ wave vectors, a well-defined θ and k_{laser} are essential. However, multiphoton photoelectric emission depends not only on the coupling efficiency, but also on the incident laser power density. Therefore a partially focused CPM laser beam is employed to couple the unamplified photon field to the SP modes. Since the width of the ATR dip of the Ag is quite small, ~0.25°, corresponding to a δk_x of 485 cm^{-1}, therefore unlike the other films, this width is sensitive to the purity of the photon wave vectors. Furthermore, this momentum wave vector impurity is also entangled with the large intrinsic δk vector, 1045 cm^{-1}, delivered by the transform-limited 90-fs-pulsed CPM laser.

The theoretical fit to the p-polarized ATR spectrum using Eq. (2) is plotted in Fig. 5 together with the normalized field density calculations based on Eqs. (4) and (5), but raised to the power $2n$ for the n-photon process, i.e., $|E_{122}+E_{12}e^{i\Psi}|^{2n}$. Good agreement between theory and experiment are found on all films except Al. Table I lists a summary of the experimental and theoretical values, where $\delta\theta_{\text{SP}}$ is defined as $\theta_{\text{SP}-R}-\theta_{\text{SP}-T}$. For Al, a shift in the peak of the electron emission towards the smaller angle of incidence by 0.95° and a substantially narrower full width at half maximum are predicted, but not observed. Since all films were exposed to air for a brief moment and electron emission is more sensitive to surface conditions than the ATR spectra, this discrepancy might be due to the oxide formation of the Al film. To account for this behavior more accurately, one might have to weigh the electron-emission process between the SP field and the ATR dip simultaneously.

B. Multiphoton photoelectric effect and electron-yield enhancement

The nonlinear behavior of the electron emission with and without SP excitation were studied by varying the input laser intensity and measuring the output electron current. The logarithmic plots shown in Fig. 6 indicate a

TABLE I. Summary of field-enhancement calculations.

	Ag	Au	Cu	Al
Film thickness (Å)	475	455	430	110
ϵ_m (fitted)	$-17.5+i0.5$	$-10.6+i0.8$	$-10.3+i1.1$	$-41+i21$
Theory $\theta_{\text{SP}-R}$ (deg)	42.88	44.13	44.29	42.90
Theory $\theta_{\text{SP}-T}$ (deg)	42.87	43.97	44.02	41.95
Theory $\delta\theta_{\text{SP}}$ (deg)	0.01	0.16	0.27	0.95
Experiment $\theta_{\text{SP}-R}$ (deg)	42.89	44.18	44.31	43.06
Experiment $\delta\theta_{\text{SP}}$ (deg)	0.01	0.28	0.19	0.28
n photon	2	3	3	3
R_{SP} (SP resonance)	0.32	0.15	0.07	0.02
$R_{\neq\text{SP}}$ (normal incidence)	0.95	0.833	0.755	0.59
Measured enhancement	3500	1000	2500	50
QE at SP at 50 MW/cm^2	10^{-7}	8×10^{-7}	0.5×10^{-7}	0.016×10^{-7}
$\left[\frac{1-R_{\text{SP}}}{1-R_{\neq\text{SP}}}\right]^n$	185	125	54.7	13.6
$\lvert E_{122}+E_{12}e^{i\Psi}\rvert$	3.89	2.66	2.34	0.81
$\lvert E_{32}+E_{322}e^{i\Psi}\rvert$	0.453	0.558	0.562	0.285
$\left\lvert\frac{E_{122}+E_{12}e^{i\Psi}}{E_{32}+E_{322}e^{i\Psi}}\right\rvert^{2n}$	5437	11735	5144	515

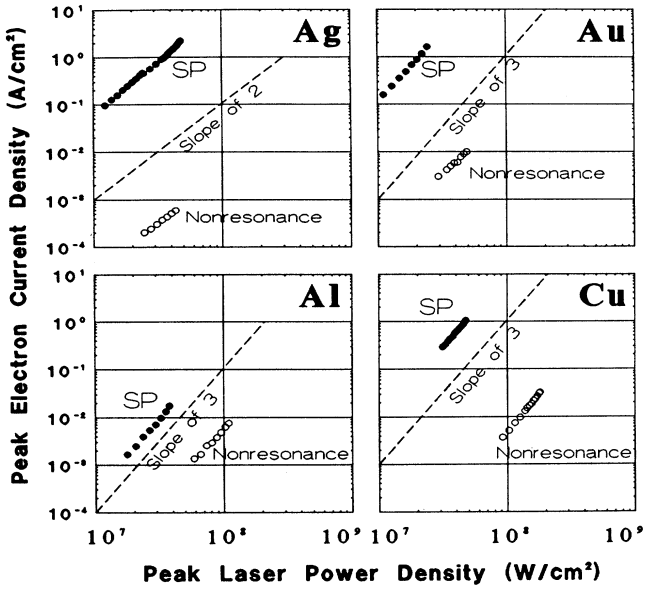

FIG. 6. Peak electron current density plotted against the peak input laser power density for Ag, Au, Al, and Cu films at SP resonance and nonresonance. The nonresonance photoemission is obtained by irradiating the laser at ~43° onto the metal film from the vacuum side.

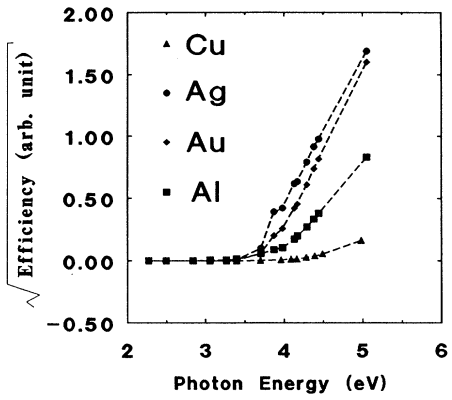

FIG. 7. Calculated total electric fields (sum of incident and reflected) across the three-layer dielectric structures for the 475-, 455-, 430- and 110-Å-thick films of Ag, Au, Cu, and Al, respectively. The solid lines are the field distributions at SP resonance, while the dashed lines are the nonresonance cases.

two-photon process for Ag film and three-photon processes for Au, Al, and Cu, regardless of the coupling conditions. The maximum electron current density achieved with the SP is ~2.5 A/cm^2, at the power density of 5×10^7 W/cm^2 from Ag. This corresponds to a quantum efficiency (QE), the number of electrons per fundamental photon, of 1×10^{-7}. Notice that the input photon energy per pulse is only ~0.2 nJ, and the QE improves linearly with input power for a two-photon process and quadratic with a three-photon process. Therefore the advantage of multiphoton photoemission is immediately clear. We should note that although electron currents reach ~10 A/cm^2 at 1 kV bias, the space-charge effect is still negligible until ~ 1 kA/cm^2.[30] The absence of a space-charge effect in this experiment can be illustrated by the linearity of the lines shown in Fig. 6, indicating the continuous flow of electrons even at the maximum laser power.

The work function of crystalline Ag is ~4.3 eV (Ref. 31) and the photon energy used is 2 eV, hence the fact that a two-photon process is observed on Ag is interesting. However, characteristics of thin metal films are different from their bulk materials. Therefore the work functions of each individual film is measured with a Xe-Hg white-light source. Results are plotted in Fig. 7 and are tabulated in Table II. Indeed the ϕ of the 475-Å-thick Ag film is only 3.65 eV, thus a two-photon process is adequate to eject an electron. However, Au and Al are also measured to have a ϕ lower than 4 eV, but a three-photon process is required. Possible explanations are surface contamination and perhaps onset of the thermally assisted photoemission.[19]

Since photoelectron emission is a single-particle excitation while SP is a collective excitation, it is conceivable that the 2-eV photons couple to the fundamental SP. Energy stored by the SP mode is then dissipated via coupling to the single-electron state, which is believed to have a rather high coupling efficiency.[32] This process results in the ejection of electrons closely resembling a regular photoemission. To understand the electron-emission process via the SP, we examine the possibility of other electron-emission channels. Under our experimental arrangement, momentum matching conditions forbid the nonlinear coupling between the photon and the second-harmonic SP.[2,33] Furthermore, electron emission due to absorption of a photon and second-harmonic generation at the metal-vacuum interface has low probability.[34] Therefore we believe that the nonlinearity of the electron

TABLE II. Multiphoton parameters and the work functions.

	Ag	Au	Cu	Al
Film thickness (Å)	475	455	430	110
n photon	2	3	3	3
Work functions (eV)	3.65	3.8	4.2	3.9
a_n with SP (cm^2/A)^n	3.2×10^{-23}	3.0×10^{-31}	2.3×10^{-32}	5.7×10^{-34}
b_n with SP (A cm$^{2(n-1)}$/MW^n)	10^{-3}	1.6×10^{-4}	8×10^{-6}	3.2×10^{-7}
$a_n\neq$SP (cm^2/A)^n	1.9×10^{-24}	2.6×10^{-32}	8.7×10^{-34}	1.5×10^{-34}
$b_n\neq$SP (A cm$^{2(n-1)}$/MW^n)	3.2×10^{-7}	8×10^{-8}	5.6×10^{-9}	6.4×10^{-9}

emission in our experiment arose from the nonlinear coupling between the SP and an individual electron. The results obtained from Fig. 6 can be used to estimate the constant a_n appearing in Eq. (7). One can then infer the electron escape probability and the multiphoton absorption coefficient b_n from the simplified form of Eq. (7). Results of these calculations for a_2 and b_2 of Ag, a_3 and b_3 of Au, Al, and Cu are tabulated in Table II. Unfortunately, literature values exist only for tungsten[19] and gold[35] at different wavelengths and input power density, therefore a direct comparison cannot be made.

The enhancement of photoelectric emission due to SP resonance is shown in Fig. 6 by comparing the electron yield at the SP resonance angle to the yield obtained by irradiating the metal films at $\sim 43°$ with the same p-polarized beam from the vacuum side. The measured electron yields are 3500, 1000, 2500, and 50 times higher than that of the nonresonance cases for Ag, Au, Cu, and Al films, respectively. Theoretically calculated electric fields using Eq. (11) are done. Figure 8 plotted the calculated total electric-field densities across the metal films when the SP's are in resonance (solid lines). For nonresonance irradiation, the total fields are also plotted (dashed lines); however, the laser beam is emerging from the vacuum side instead. To evaluate the enhancement factor based on the SP field, we calculate the ratio of the total field of each film raised to the $2n$ power at the metal side of the metal-vacuum boundary. The magnitude of these electric fields are also reproduced in Table I. A comparison of the enhancements between theory and experiment indicates that enhancements based on reflectivity measurements are not as reliable as the field calculations. However, field density calculations seem to have overestimated the enhancement, while reflectivity measurements have underestimated it.

C. Electron temporal response

The electron temporal profiles are measured on different metal films utilizing the multiphoton photoelectric effect. Unlike semiconductor photocathodes,[36] the temporal response of a metal photocathode is believed to be limited only by the existence of surface states and the transit time for the electrons to diffuse to the metal surface. Real-time measurements of the electron pulse duration become almost impossible in the femtosecond time regime. However, nonlinear photoemission employing two collinear femtosecond laser beams is in fact a higher-order correlation. Therefore the correlated electron yield gives directly the electron pulse duration when they are spatially and temporally overlapping on the metal surface.

The results of these measurements on all four metal films are depicted in Fig. 9. The electron high-order correlated temporal profiles strikingly resemble that of the laser autocorrelations. The agreements of the Ag film are reasonable because both the laser autocorrelation and the multiphoton emission are second order. However, the multiphoton electron emission from Au, Cu, and Al is a third-order process (see Fig. 6), therefore the intrinsic electron temporal profile should be narrower than the laser autocorrelation by a factor of $\sqrt{3/2}$, assuming Gaussian pulses. More studies are required to fully understand this discrepancy.

It has been speculated that some fraction of photoelectrons emitted from metals originate from a thin layer of metal surface.[37] These photoelectrons might have suffered electron-electron collisions. According to dc conductivity measurements, the electron-electron scattering time is ~ 30 fs. The laser pulses employed in this ex-

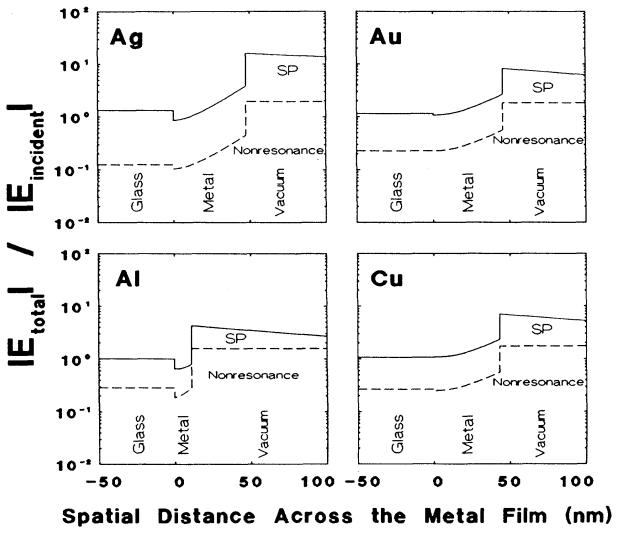

FIG. 8. Work functions of the thin films used in this study. The measurements are done using a Xe-Hg white-light source.

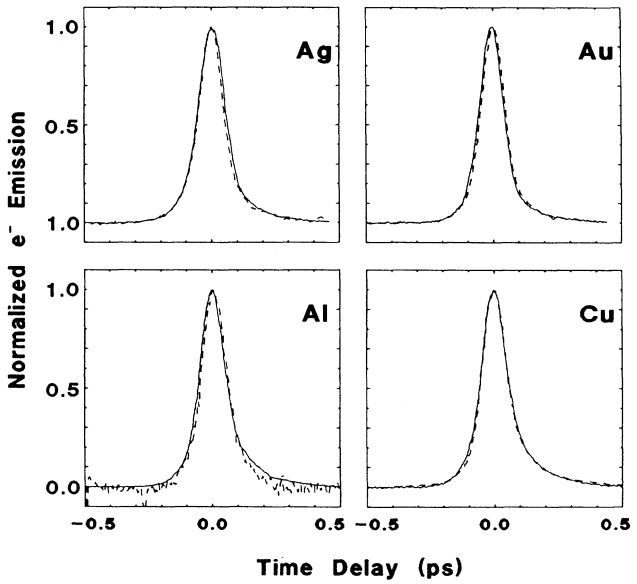

FIG. 9. Electron temporal profiles (solid lines) using multiphoton photoemission and the corresponding laser autocorrelations (dashed lines) from second-harmonic generation from a 100-μm-thick potassium dihydrogen phosphate crystal.

periment are ~90 fs; therefore, if photoelectrons have suffered collision, a broadened electron temporal profile would have resulted. But the fact that no noticeable broadening is observed leads us to conclude that the majority of the photoelectrons do not suffer any electron-electron collisions. The absence of this temporal broadening also reveals that no thermally assisted photoemission is occurring,[19] and the temperature of the nonequilibrium electrons[38,39] did not contribute any significant photoelectrons.

V. CONCLUSIONS

In conclusion, a two-photon-like photoemission from a 475-Å-thick Ag film and a three-photon-like process from films of 455-Å-thick Au, 430-Å-thick Cu, and 110-Å-thick Al are found when they are irradiated by a 2-eV photon source. When photons are coupled resonantly to the SP modes, electron-yield enhancement of 3500, 1000, 2500, and 50 higher than that of the bulk emission measured for the same film at the same power fluence are observed from Ag, Au, Cu, and Al, respectively. QE's of 10^{-7}, 8×10^{-7}, 0.5×10^{-7}, and 1.6×10^{-9} are obtained from SP-mediated electron emission from Ag, Au, Cu, and Al films, respectively, at the input power density of 50 MW/cm^2. Based on a theoretical investigation, we found the nature of the enhancement favors the localized SP field calculations using the Fresnel coefficients rather than the absorption relying on the reflectivity measurements. By monitoring the electron current and the reflectivity simultaneously, we have shown that electron emission peaked at a slightly different incident angle than that registered by the ATR spectra, which was predicted by the SP field calculations. We have also demonstrated the electron-pulse duration measurement in the femtosecond time regime using the nonlinear photoelectric effect. The electron pulse durations are found to be only limited by the laser. However, the width of the electron pulses fail to narrow, commensurate with a higher-order autocorrelation.

In the SP-enhanced electron scheme, the electrons are ejected in a forward direction with respect to the laser beam, thereby reducing the possible interaction of the electrons with the intense photon field and consequently suppressing electron momentum broadening.[40] The maximum SP field density at the metal-vacuum interface could ensure a larger fraction of the photoelectrons escaping to the vacuum, and the nonequilibrium of hot electrons generated using the ultrashort laser pulses may provide a condition favorable for the creation of a ballistic-type high current density electron beam. The upper limit of the peak electron current density, however, is governed by the damage threshold of the thin metal films. This precious information remains to be explored at the femtosecond time regime.

ACKNOWLEDGMENTS

We would like to acknowledge the support of Dr. Veljko Radeka and Dr. Robert Palmer. We thank Dr. Robert Dinardo for the preparation of the metal films. We appreciate the expert technical assistance of Niel Schaknowski and John Schill.

[1]H. J. Simon, D. E. Mitchell, and J. G. Watson, Phys. Rev. Lett. **33**, 1531 (1974).
[2]J. C. Quail, J. G. Rako, H. J. Simon, and R. T. Deck, Phys. Rev. Lett. **50**, 1987 (1983).
[3]T. Tsang and D. D. Smith, Opt. Commun. **70**, 115 (1989).
[4]A. L. Moretti, W. M. Robertson, B. Fisher, and R. Bray, Phys. Rev. B **31**, 3361 (1985).
[5]W. M. Robertson, A. L. Moretti, and R. Bray, Phys. Rev. B **35**, 8919 (1987).
[6]*Surface Enhanced Raman Scattering,* edited by R. K. Chang and T. E. Furtak (Plenum, New York, 1982).
[7]J. B. D. Soole, R. N. Lamb, and H. P. Huges, Solid State Commun. **59**, 607 (1986).
[8]S. Ushioda, J. E. Rutledge, and R. M. Pierce, Phys. Rev. B **34**, 6804 (1986).
[9]P. Martinot, A. Koster, and S. Laval, IEEE J. Quantum Electron. **QE-21**, 1140 (1985).
[10]S. M. Arakelian *et al.*, Phys. Lett. A **145**, 49 (1990).
[11]J. Bösenberg, Phys. Lett. **37A**, 439 (1971).
[12]Ch. Macek, A. Otto, and W. Steinmann, Phys. Status Solidi B **51**, K59 (1972).
[13]H. K. Rudolf and W. Steinmann, Phys. Lett. **61A**, 471 (1977).
[14]G. Hincelin, Phys. Rev. B **24**, 787 (1981).
[15]T. Tsang, T. Srinivasan-Rao, and J. Fischer, Opt. Lett. **15**, 866 (1990).
[16]R. L. Smith, Phys. Rev. **128**, 2225 (1962).
[17]J. H. Bechtel, W. Lee Smith, and N. Bloembergen, Phys. Rev. B **15**, 4557 (1977).
[18]S. I. Anisimov, V. A. Benderskii, and G. Farkas, Usp. Fiz. Nauk **122** (2), 185 (1977) [Sov. Phys.—Usp. **20** (6), 467 (1977)].
[19]R. Yen, J. Liu, and N. Bloembergen, Opt. Commun. **35**, 277 (1980).
[20]Gy. Farkas *et al.*, J. Appl. Phys. **62**, 4545 (1987).
[21]J. T. Stuckless and M. Moskovits, Phys. Rev. B **40**, 9997 (1989).
[22]Gy. Farkas and Cs. Tóth, Phys. Rev. A **41**, 4123 (1990).
[23]E. Kretchmann, Z. Phys. **241**, 313 (1971).
[24]U. Fano and L. Fano, *Physics of Atoms and Molecules: An Introduction to the Structure of Matter* (The University of Chicago Press, Chicago, 1972), pp. 31–40.
[25]R. D. Olney and R. J. Romagnoli, Appl. Opt. **26**, 2279 (1987).
[26]E. F. Y. Kon and T. Tamir, Appl. Opt. **27**, 4098 (1988).
[27]J. C. Dudek, Rev. Phys. Appl. **13**, 387 (1978).
[28]J. H. Bechtel, W. L. Smith, and N. Bloembergen, Phys. Rev. B **15**, 4557 (1977).
[29]P. B. Johnson and R. W. Christy, Phys. Rev. B **6**, 4370 (1972).
[30]R. Clauberg and A. Blacha, J. Appl. Phys. **65**, 4095 (1989).
[31]M. Chelvayohan and C. H. B. Mee, J. Solid State Phys. C **15**, 2305 (1982).
[32]T. E.Furtak and J. K. Sass, Surf. Sci. **78**, 591 (1978).
[33]F. De. Martini, P. Ristori, E. Santamato, and A. C. A. Zam-

mit, Phys. Rev. B **23**, 3797 (1981).
[34]J. C. Quail and H. J. Simon, Phys. Rev. B **31**, 4900 (1985).
[35]E. M. Logothetis and P. L. Hartman, Phys. Rev. Lett. **18**, 581 (1967).
[36]K. Kinoshita, M. Ito, and Y. Suzuki, Rev. Sci. Instrum. **58**, 932 (1987).
[37]S. V. Pepper, J. Opt. Soc. Am. **60**, 805 (1970).
[38]J. G. Fujimoto, J. M. Liu, E. Ippen, and N. Bloembergen, Phys. Rev. Lett. **53**, 1837 (1984).
[39]R. W. Schoenlein, W. Z. Lin, J. G. Fujimoto, and G. L. Eesley, Phys. Rev. Lett. **58**, 1680 (1987).
[40]E. Yablonovitch, Phys. Rev. Lett. **60**, 795 (1988).